# Cooperative adsorbate binding catalyzes high-temperature hydrogen oxidation on palladium

**Authors:** Michael Schwarzer<sup>1,2</sup>, Dmitriy Borodin<sup>1,2</sup>†, Yingqi Wang<sup>3</sup>, Jan Fingerhut<sup>1</sup>, Theofanis N. Kitsopoulos<sup>2,4</sup>, Daniel J. Auerbach<sup>2</sup>, Hua Guo<sup>3</sup> and Alec M. Wodtke<sup>1,2,5</sup>\*

# **Affiliations:**

<sup>1</sup>Institute for Physical Chemistry, University of Göttingen; 37077 Göttingen, Germany.

<sup>2</sup>Department of Dynamics at Surfaces, Max Planck Institute for Multidisciplinary Sciences; 37077 Göttingen, Germany.

<sup>3</sup>Department of Chemistry and Chemical Biology, Center for Computational Chemistry, University of New Mexico; Albuquerque, NM 87131, USA.

<sup>4</sup>School of Mathematics and Natural Sciences, University of Southern Mississippi; Hattiesburg, MS 39406, USA.

<sup>5</sup>International Center for Advanced Studies of Energy Conversion; 37077 Göttingen, Germany.

\*Corresponding author. Email: <u>alec.wodtke@mpinat.mpg.de</u>

†present address: Center for Quantum Nanoscience, Ewhayeodae-gil 52, Daehyeon-dong, Seodaemun-gu, 03760 Seoul, South Korea.

20

5

10

15

25

**Abstract:** Atomic-scale structures that account for the acceleration of reactivity by heterogeneous catalysts often form only under reaction conditions of high temperatures and pressures, making them impossible to observe with low-temperature, ultrahigh vacuum methods. We present velocity-resolved kinetics measurements for catalytic hydrogen oxidation on Pd over a wide range of surface concentrations and at high temperatures. The rates exhibit a complex dependence on oxygen coverage and step density that – using density functional and transition-state theories – can be quantitatively explained by a kinetic model involving a cooperatively stabilized configuration of at least three O-atoms at steps. Here, two O-atoms recruit a third O-atom to a nearby binding site to produce an active configuration that is far more reactive than isolated O-atoms. Thus, hydrogen oxidation on Pd reveals a clear example of how reactivity can be enhanced on a working catalyst.

5

10

One sentence summary: Hydrogen oxidation on Pd is catalyzed by an active configuration involving cooperative binding of both O and Pd atoms.

Since the early 1800's, when Döbereiner first amazed the public and fellow natural philosophers by oxidizing hydrogen over a platinum sponge to create "fire without flint and tinder" (1, 2), heterogeneous catalysis has revolutionized chemistry. Platinum-group metal catalysts in particular have proven to be some of the most important materials in modern industry (3). Applications include: the catalytic removal of pollutants from combustion (4, 5), hydrogen production and purification (6, 7), catalytic fuels cells (8-10), chemical catalysis (11-13) and, in particular, the production of artificial fertilizers (14, 15). Despite its importance, we still lack a mechanistic understanding of most reactions in heterogeneous catalysis.

To appreciate the challenges involved, consider that gas-phase reactivity occurs within a homogeneous environment and depends only on the relative positions and velocities of the reacting atoms, but in heterogeneous catalysis, reactivity also depends on the positions of the reactants with respect to a catalytic surface. For example, even on single crystal surfaces – the most homogeneous catalysts one can produce in the laboratory – reactions often occur selectively at a tiny minority of step "defect" sites where low-valence metal atoms are present (16, 17). The concept of active sites has thus become central to our thinking about surface chemistry, and they can sometimes be identified on pristine crystalline surfaces using low-temperature microscopy (18).

Unfortunately, there is no general way to determine the nature of active sites at the high temperatures and pressures typical of real catalysis. There is also evidence that barrier heights and the energies of reaction intermediates can be influenced by so-called spectator adsorbates (19, 20). Adding to the challenge, real catalytic surfaces operating at high temperatures and pressures are hardly pristine and may exhibit reactive structures — what we call active configurations — that may not even exist under nonreactive conditions. Hence, determining the properties of active configurations present on dynamic catalysts (21-24) operating under reacting conditions is an important challenge in modern surface chemistry (25).

Here, we report high-precision velocity-resolved kinetics (VRK) (26, 27) measurements over a wide range of coverages and temperatures, as well as results from theoretical kinetics involving density functional theory (DFT) and transition-state theory (TST), that reveal the mechanism of hydrogen oxidation on palladium catalysts. The reaction involves an active configuration of cooperatively-bound oxygen atoms that forms along a palladium step and only under conditions with elevated oxygen concentrations. At reduced oxygen concentrations, the reaction slows dramatically and the kinetic order changes. These results show how reactivity can be enhanced on a working catalyst operating under reacting conditions.

#### **Background**

5

10

15

20

25

30

35

We outline what has been known about the kinetics of this reaction prior to this study. The overall reaction can be formally written as

$$0_{2(g)} + 2H_{2(g)} \xrightarrow{Pd} 2H_2O_{(g)}$$
,

where activated forms of  $H_{2(g)}$  and  $O_{2(g)}$  are first produced by dissociative adsorption. Subsequently, the atoms recombine to form thermodynamically stable water (28-30). Only a few elementary reactions are possible.

$$O_{2(g)} + 2 * \xrightarrow{k_1} 2 O^* \tag{1}$$

$$H_{2(g)} + 2 * \stackrel{k_2}{\rightleftharpoons} 2 H^*$$
 $k_{-2}$  (2)

$$H^* + O^* \stackrel{k_3}{\rightleftharpoons} OH^* + *$$
 $k_{-3}$ 
(3)

$$\begin{array}{c}
k_5 \\
2 \text{ OH}^* \rightleftharpoons \text{H}_2 \text{O}^* + \text{O}^* \\
k_{-5}
\end{array} \tag{5}$$

$$H_2O^* \stackrel{k_6}{\to} H_2O_{(g)} + *$$
 (6)

All prior studies suggest that reaction (3) is rate-limiting. However, the derived activation energies differ widely from one another (0.3 to 0.8 eV) (31-33). A comparison to electronic structure calculations, which predict a barrier to  $OH^*$  formation of  $\sim 1$  eV and that reaction (5) is barrier-less on a defect-free Pd(111) surface (34, 35), suggests that the rate of reaction may depend strongly on details of the experimental conditions such as the step density of the catalyst. Beyond this, the relative importance of reactions (4) and (5) has remained unknown (31, 33, 36).

# **Experimental results**

5

10

15

20

25

Figure 1 shows representative water formation rates (left panels) obtained with VRK; here, two pulsed molecular beams and a leak valve were available for pulsed and continuous reactant deposition and a high power short pulsed laser was used for non-resonant multi-photon ionization of desorbed products. Ion-imaging provided velocity-resolved product detection (26, 27). See sec. S1 for additional experimental details. Results are presented under oxygen rich (A, B, and C) and lean (D, E, and F) conditions as well as for low (•) and high (•) Pd step densities. The reaction is unexpectedly complex. For oxygen-rich conditions, it proceeds much faster on a surface with high step density (Fig. 1A), whereas for oxygen-lean conditions (Fig. 1D), the reaction was much slower and depends only weakly on step density. Even the order of the reaction kinetics changed. Second-order reactions were seen under oxygen rich conditions (Fig. 1B), whereas pseudo 1<sup>st</sup> order kinetics were seen for oxygen-lean conditions (Fig. 1E). Based on these observations, secondorder reaction rate constants were derived from basic kinetics assumptions (Fig. 1C and F). For oxygen rich conditions—where a pulse of H<sub>2</sub> impinges onto an O-covered surface—we assumed that all H<sub>2</sub> molecules from the molecular beam undergo an A+A type second-order reaction to yield the observed transient shape (see sec. S2 for more detail). For oxygen lean conditions where a pulse of O<sub>2</sub> impinges on an H-covered surface—we applied pseudo first-order conditions for the H-atom coverage to obtain reaction rate constants. See section S3 of the SI for additional detail.

# **Comparison with DFT results**

These observations suggested that the rate-limiting reaction changed with oxygen coverage. For oxygen-rich conditions (Fig. 1C), the experimentally derived activation energies of  $0.44 \pm 0.02$  eV on Pd(111) and  $0.50 \pm 0.01$  eV on Pd(332) compared well with our DFT-computed barrier

heights using two functionals (RPBE: 0.43 eV, PBE: 0.40 eV) for the OH\*disproportionation – reaction (5) – occurring at steps (see Table S8). This result also explained the second-order kinetics.

For oxygen-lean conditions, the experimentally derived activation energies of  $0.80 \pm 0.01$  eV on Pd(111) and  $0.80 \pm 0.01$  eV on Pd(332) were similar to DFT predicted barrier heights (RPBE: 0.93 eV, PBE: 0.93eV) for OH\* formation at steps, a reaction that we expected to exhibit pseudo-first-order kinetics under our experimental conditions. We concluded that the rate-limiting step for water formation under oxygen-lean conditions was OH\* formation occurring at steps, whereas OH\* disproportionation occurring at steps was rate-limiting under oxygen-rich conditions.

5

10

15

20

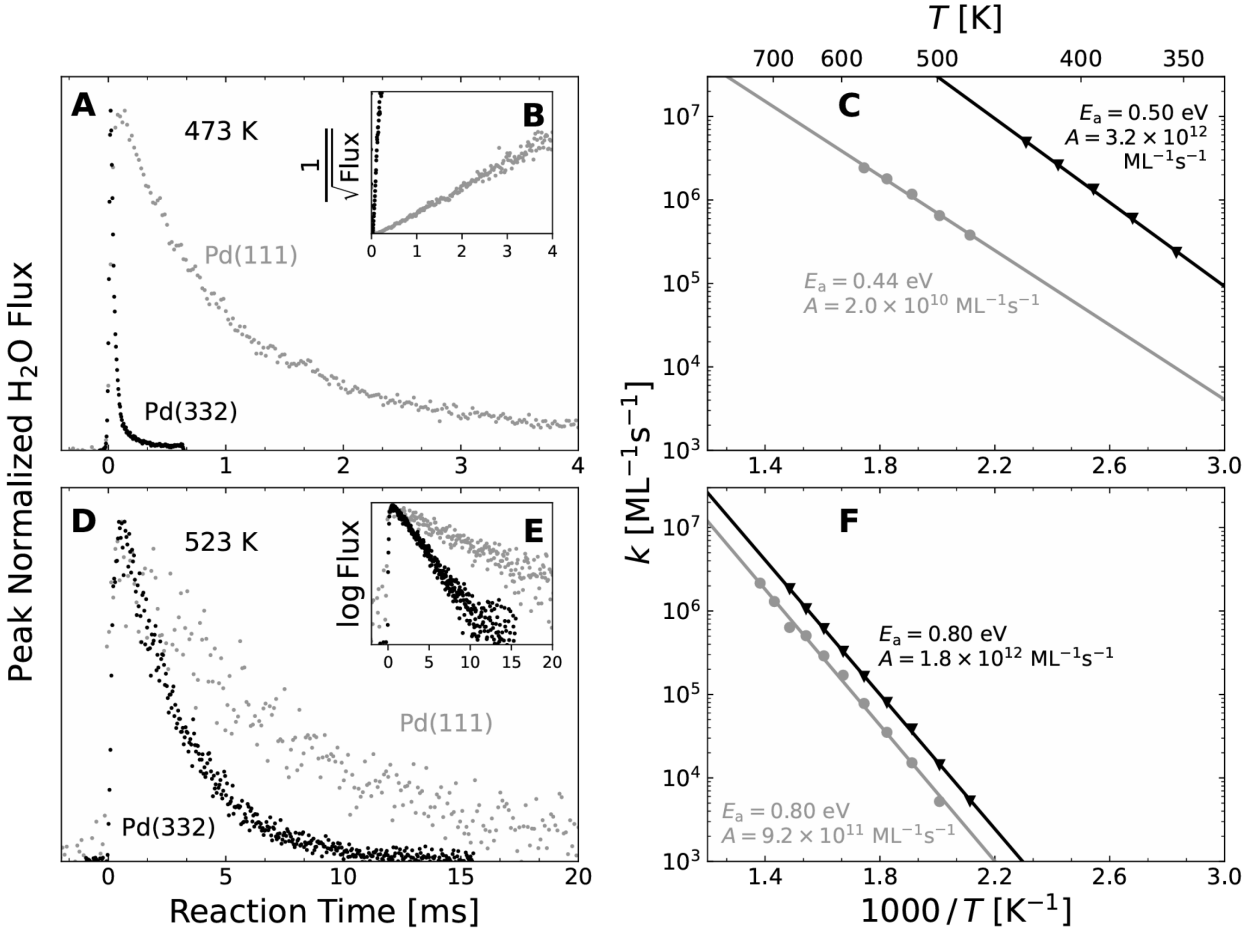
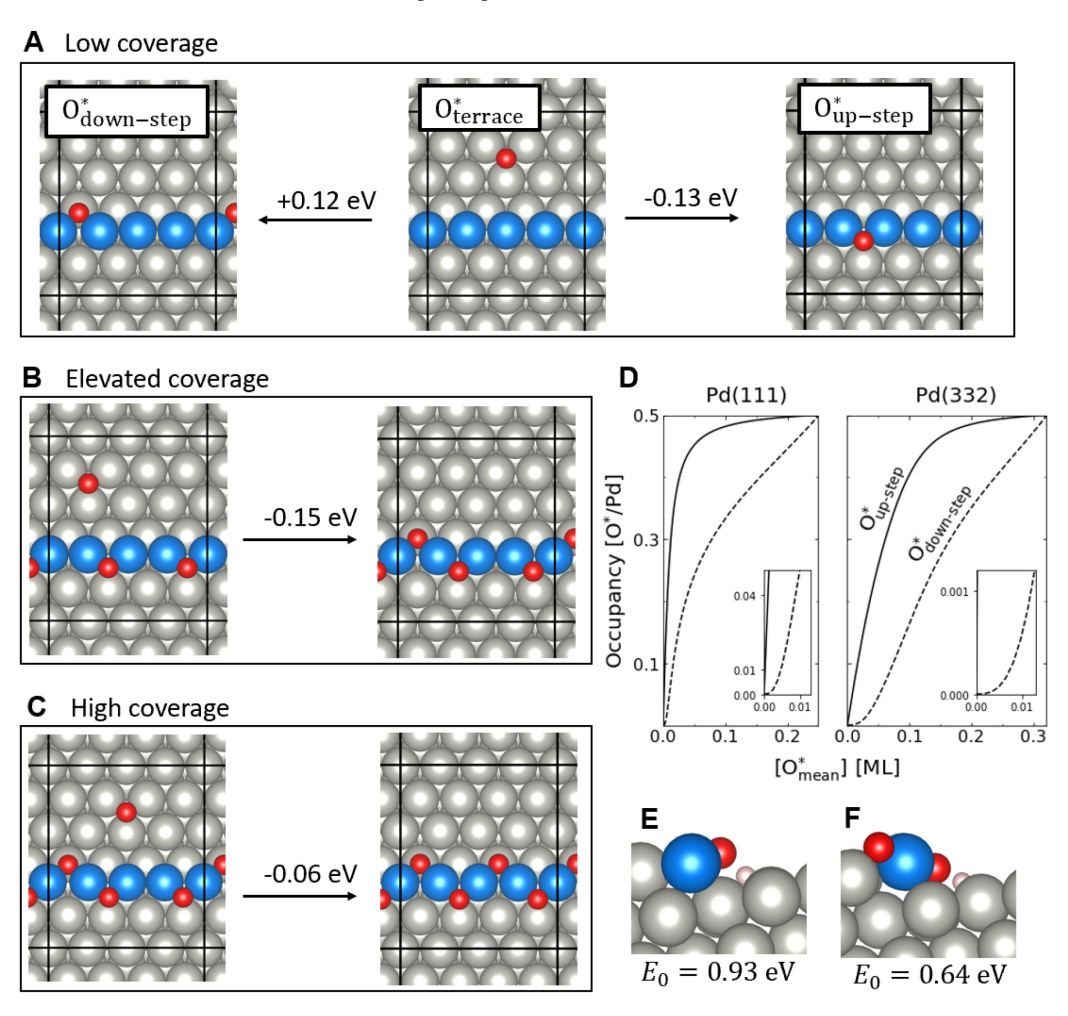


Fig. 1. The kinetics of catalytic hydrogen oxidation on Pd: Dependence on oxygen coverage, step density and temperature. (A) Experimentally observed water formation rates for Pd (332) ( $\bullet$ ) and (111) ( $\bullet$ ) at 473 K for  $[O^*_{mean}] = 0.03$  ML. We define 1 monolayer (ML) as the coverage corresponding to a one-to-one ratio of adsorbate molecules to Pd surface atoms. The H-atom coverage  $[H^*]$  is limited by the dose (0.002 ML) of the reaction initiating H<sub>2</sub> pulsed beam. Inset (B) shows a 2<sup>nd</sup> order linearization of the rate data – see also Fig. S3. (C) Arrhenius plots of the rate constants obtained from data as shown in panel (A). (D) Same as panel (A) but  $[H^*] = 0.026$  ML and the  $[O^*_{mean}]$  is limited by the dose (0.001 ML) of the reaction initiating O<sub>2</sub> pulsed beam. Inset (E) shows a 1<sup>st</sup> order linearization of the rate data. (F) Arrhenius plots of the rate constants obtained from data of panel (D).

The rate-limiting reaction changing with increasing oxygen coverage suggested that reactions of isolated 0\* atoms that are important under oxygen-lean conditions could not explain reactivity at higher coverage. Figure 2 shows results of DFT calculations carried out on a 4x1 unit cell with periodic boundary conditions – computational details are presented in sec. S4 – that provided insights into how the rate-limiting reaction could change with O coverage. Figure. 2 A depicts 0\* structures on a Pd (332) surface in the isolated-atom limit. Here, 0\* binds most favorably above a

face-centered cubic (fcc) hollow site next to a monatomic step, hereafter referred to as  $O^*_{up-step}$ , and somewhat less stably at the fcc hollow sites of the (111) terrace, hereafter referred to as  $O^*_{terr}$ . Binding at the fcc face of the (111) step, hereafter referred to as  $O^*_{down-step}$ , was unstable with respect to  $O^*_{terr}$  or  $O^*_{up-step}$ . However, as can be seen in Fig. 2B,  $O^*_{down-step}$  became stable in the presence of two neighboring  $O^*_{up-step}$  atoms.



5

10

15

Fig. 2. Theoretical predictions of cooperative binding of  $O^*$  on the stepped Pd(332) surface. (A) In the isolated atom limit  $O^*_{up-step}$  is bound most strongly. (B) At higher oxygen coverage, the  $O^*_{up-step}$  occupation rises, increasing the probability to find  $O^*_{up-step}$  neighbours, which stabilize the binding of  $O^*_{down-step}$ . (C) The cooperative stabilization energy is reduced as the steps become saturated. The black lines show the unit cell defining the periodic boundary conditions used in the DFT calculations. (D) Equilibrium populations of  $O^*_{up-step}$  and  $O^*_{down-step}$  versus mean  $[O^*]$  for Pd (332) and (111) at 473 K. The step densities of the (111) and (332) surfaces are 0.2% and 16.7%, respectively. (E) Transition state of OH formation at  $O^*_{up-step}$  and (F) at  $O^*_{down-step}$ . Terrace Pd atoms are shown in grey, step Pd atoms in blue, O atoms in red and H atoms in pink. Calculations were done using RPBE.

These cooperative interactions suggested that at increased oxygen coverage, a "zigzag" O-decorated Pd step structure (Fig. 2 C) could form, similar to one that has been previously studied (37, 38). Of great consequence to the reactivity, the barrier for OH\* formation was substantially lower for reaction at O\*<sub>down-step</sub> (RPBE: 0.64 eV, PBE: 0.60 eV) compared to reaction at O\*<sub>up-step</sub> (RPBE: 0.93 eV, PBE: 0.93 eV). We hypothesize that the OH disproportionation reaction became

rate limiting under oxygen-rich conditions because the barrier to OH formation was reduced by the presence of  $O_{down-step}^*$ , formed through cooperative O-atom binding at Pd steps.

We next computed equilibrium populations of  $O^*_{down-step}$  and  $O^*_{up-step}$  as a function of  $[O^*_{mean}]$  and T using the kinetic model introduced below. Figure  $2\mathbf{D}$  shows that the population of  $O^*_{down-step}$  was important at all but the lowest mean coverages. It grew as  $[O^*_{mean}]^2$  at low  $[O^*_{mean}]$ , because two  $O^*_{up-step}$  in close proximity to one another were needed to stabilize  $O^*_{down-step}$ . These results showed that  $O^*_{down-step}$  exhibited higher reactivity toward  $OH^*$  formation and was present in sufficient abundance, which made it a candidate for the cooperatively formed active configuration hypothesized above.

# Mechanism and Kinetic modelling

We next present a reaction mechanism involving cooperative O-atom binding to obtain TST rate constants based on DFT energies and vibrational frequencies (see secs. S4-S8 for details). Figure 3 shows the potential energy diagram for water formation. The lowest energy pathway from reactants to products for oxygen-lean conditions formed OH\* through reaction of H\* with  $O^*_{up-step}$ , whereas under oxygen-rich conditions, H\* reacted with  $O^*_{down-step}$ . In both cases, newly formed OH\* was strongly bound at Pd steps and could undergo disproportionation to produce H<sub>2</sub>O.

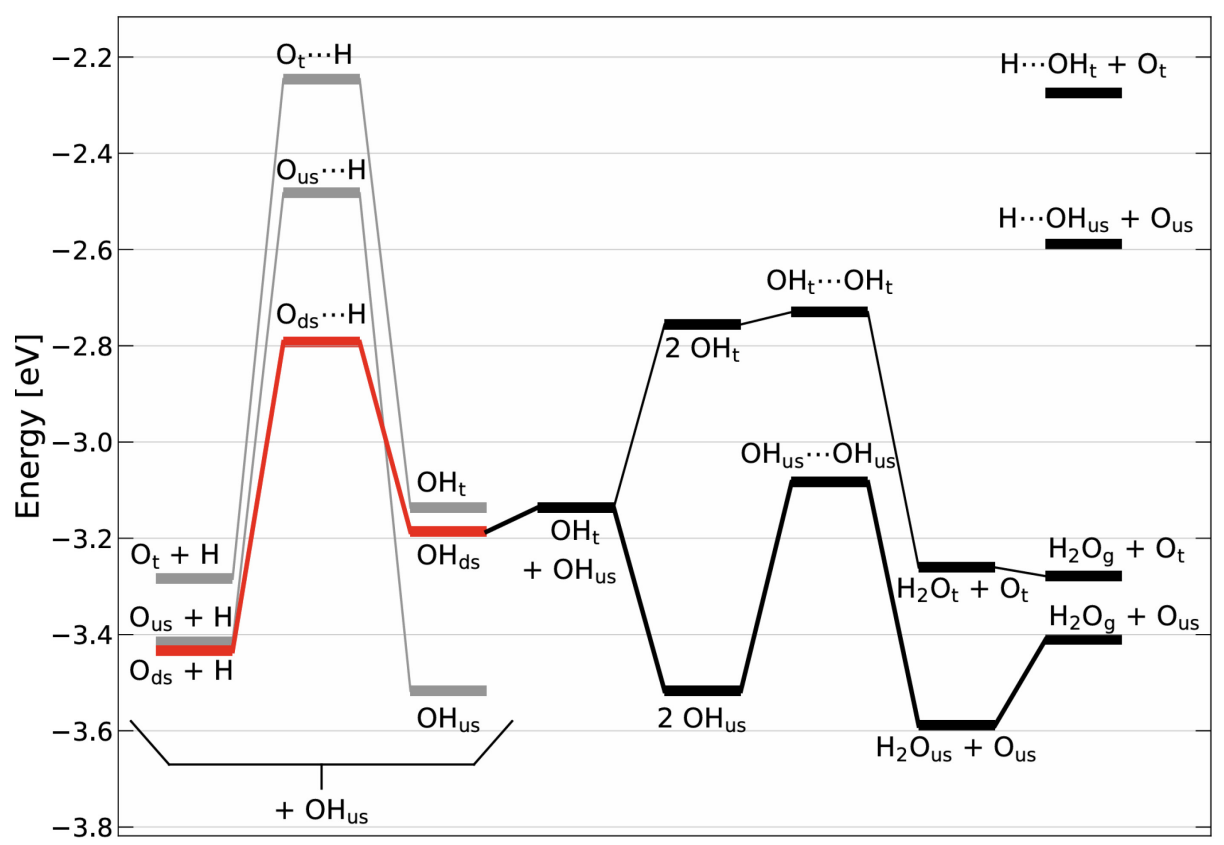


Fig. 3. Reaction paths involved in the Pd catalysed conversion of hydrogen and oxygen to water. The dominant reaction flux on Pd(332) at elevated O-coverages (drawn in red) involves  $OH^*$  formation at the  $O_{down-step}^*$  site, diffusion of  $OH^*$  to terraces and subsequent trapping at steps, followed by disproportionation to form water. At low O-coverages,  $OH^*$  is formed at the  $O_{up-step}^*$  site. The energy of an additional  $OH_{up-step}^*$  adsorbate molecule has been added to all energies along the  $OH^*$  formation pathway to ensure mass balance in the subsequent disproportionation reaction. See also Fig. S9. For comparison, the transition-state energies for the OH + H reaction are also shown. All

5

10

structures used to construct this diagram can be found in Tables S5-S7. These results were obtained with the RPBE functional – similar results for the PBE functional can be found in the SI. The zero of energy refers to gas phase reactants and all energies are ZPE corrected. Note that down-step, up-step and terrace are abbreviated ds, us and t, respectively.

5

10

15

20

25

30

Figures 4A (oxygen-rich) and 4B (oxygen-lean) show that the TST model's predictions based on both RPBE (—) and PBE (—) input data were similar to experiment ( $\bullet$ ) – comparisons to all experimental data can be found in sec. S9 of the SI. Figure 4A also shows that neglect of OH\* formation at  $O_{\text{down-step}}^*$  (---) resulted in unrealistically slow water formation rates under oxygen-rich conditions. Figure 4B shows OH\* formation at  $O_{\text{down-step}}^*$  was unimportant under oxygen-lean conditions. A systematic degree-of-rate-control (DRC) analysis (39, 40) of the DFT/TST based mechanism (see sec. S10) showed that under oxygen-rich conditions, water production rates were sensitive to the OH\* formation rate at  $O_{\text{down-step}}^*$  and the OH\* disproportionation rate at step sites. Under oxygen-lean conditions, the water production rate was sensitive only to OH\* formation at  $O_{\text{up-step}}^*$ .

This DRC analysis of the kinetic model informed us which energies in Fig. 3 most influenced the experimental kinetic traces. As shown in Fig. 4, C and D, adjusting these energies by not more than 0.15 eV led to quantitative agreement between the kinetic model (—) and experiment (•) under both oxygen-rich and oxygen-lean conditions. Section S11 of the SI explains the fitting procedure and shows comparisons of experimental and simulated kinetic traces of the optimized model over a wide range of coverages ( $10^{-4}$  ML < [ $0^*$ ] < 0.2 ML) and temperatures (353 K <  $T_S <$  873 K). Different adjustments were made for oxygen-lean (Table S14) and oxygen-rich (Table S15) conditions to account for repulsive interactions between OH\* and O\* that are neglected in the DFT energies of the kinetic model. Such interactions can be important under oxygen-rich conditions and are assumed to be absent under oxygen lean conditions. These effects are discussed at length in sec. S12.

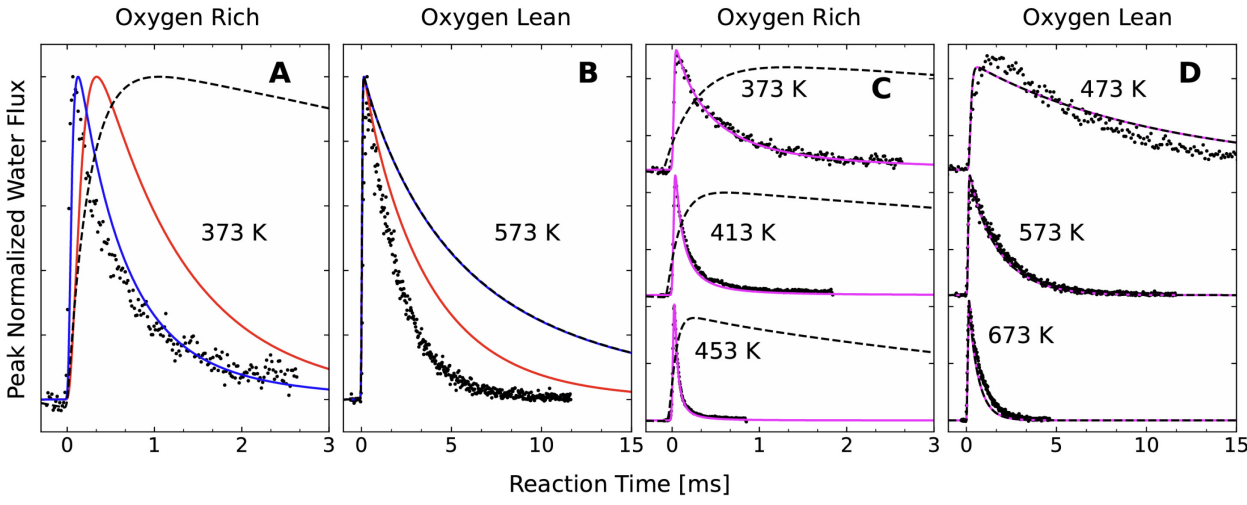


Fig. 4: Comparison of experimental and theoretical kinetic traces for water formation in hydrogen oxidation on Pd (332): Velocity-resolved kinetics results ( $\bullet$ ), TST microkinetic model based on RPBE (——), PBE (——), and the optimized model (——). For PBE and the optimized model, results are also shown neglecting reactivity at the down-step O atom (----). A)  $[O^*_{mean}] = 0.09$  ML. B)  $[H^*] = 0.003$  ML. C)  $[O^*_{mean}] = 0.09$  ML. D)  $[H^*] = 0.026$  (T = 473 K), 0.003 (T = 573 K), and 0.0007 ML (T = 673 K). For A and C, the H-coverage is limited by the dose (0.002 ML) of the reaction initiating  $O_2$  pulsed beam. For B and D, the O-atom coverage is limited by the dose (0.001 ML) of the reaction initiating  $O_2$  pulsed beam. We define one ML as the coverage corresponding to a one-to-one ratio of adsorbate molecules to Pd surface atoms.

A comprehensive comparison of the optimized model to experiment over all experimental conditions is possible using effective rate constants (as explained in sec. S2 and S3) and is shown in Fig. 5. Under oxygen lean conditions, the model reproduces the pseudo-first order values of  $k_{eff}$  and their linear dependence on hydrogen coverage. Under oxygen-rich conditions, the peculiar dependence of the second order  $k_{eff}$  on O-atom coverage is captured by the optimized model. The maximum rate constant on Pd(332) appears at somewhat higher O-coverages in the model compared to experiment. Despite these modest differences, the optimized model captures the peculiar step and O-coverage dependence seen in experiment.

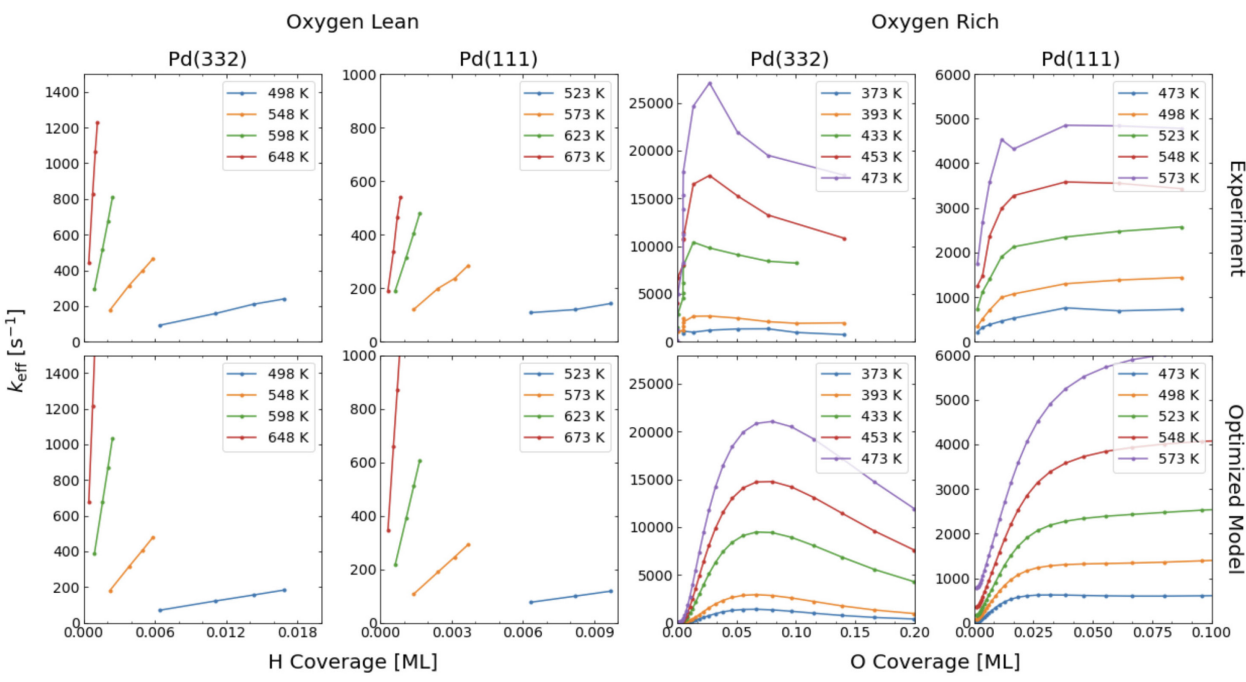


Fig. 5: Behaviour of effective rate constants  $k_{eff}$  as a function of coverage (see sec. S2 and S3). Shown are oxygen lean conditions as a function of H-atom coverage (left half) and oxygen rich conditions as a function of O-atom coverage (right half). The upper row shows effective rate constants obtained from experimental traces which compare well with effective rate constants obtained from traces of the optimized kinetic model, shown in the lower row.

#### Discussion

5

10

15

20

25

This work answers basic questions concerning the elementary reactions responsible for the catalytic conversion of hydrogen and oxygen to water on Pd. It shows that at O-coverages of  $\sim 10^{-3}$  ML, OH formation was the rate-limiting step to water formation, whereas at higher coverages, the barrier to this reaction dropped and made OH disproportionation the rate-limiting reaction. This peculiar change in kinetic mechanism resulted from the formation of an active configuration by cooperative binding of multiple O-atoms at Pd steps. This active configuration dominated the reaction under nearly all conditions; indeed, it is remarkable that conditions where it was unimportant arose only at very low O-coverages on the order of 0.001 ML.

The evidence for our conclusions came from a comparison of experimentally obtained and theoretically derived kinetics, which were in quantitative agreement with one another after DFT-computed energies along the reaction path were adjusted by up to  $\pm 0.15$  eV. These adjustments are justified given uncertainties related to the use of DFT. Specifically, computed energies may vary by up to 0.2 eV depending on choice of functional (41) and the choice of unit cell size enforces specific and high adsorbate coverages. For example, the calculations of this work used to compute

cooperative O-atom binding correspond to 0.125 and 0.167 ML – see Fig. 2 **B** and **C** – but were used to construct a kinetic model for much lower coverages as well. A discussion of these issues is provided in sec. S6, where we show that low coverage calculations yield similar results for the formation of down-step O-atoms. Furthermore, our model is a simplified micro-kinetic model with an equilibrium assumption to obtain the site-specific O-atom populations and neglects OH\* interactions with O\*. Future work, using the kinetic Monte Carlo approach would allow us to go beyond these approximations and provide an improved treatment of adsorbate-adsorbate interactions. It would also be desirable to go beyond the harmonic approximation and to include tunneling in TST calculations. Despite these limitations, our kinetic model achieved quantitative agreement with observation over a wide range of conditions. Most importantly, the kinetic model described the peculiar dependence of the observed kinetics on oxygen coverage, by means of a cooperatively bound active configuration, whose abundance is strongly dependent on  $[O^*_{mean}]$ .

results also provided a test of DFT implemented at the GGA level for calculating reaction barriers in catalysis, where few direct comparisons between experiment and theory have been possible. Although DFT-GGA involves intrinsic energy errors on the order of 0.2 eV, much larger errors can arise from an incorrect hypothesis about the structures of active configurations. In this work, finding the correct structures of the transition states of the rate limiting steps was much more important than a "correct" choice of functional. This suggests that the field may use DFT-GGA with guarded optimism, for example by developing new DFT-GGA based discovery-tools for active configurations formed due to cooperative adsorbate interactions.

Cooperative adsorbate binding is seldom discussed in heterogeneous catalysis; but, it is well known in other fields, for example in biochemistry, where the docking of one ligand enhances affinity for a second ligand (42, 43). Such behavior was first recognized through the non-linear dependence of binding site occupation on ligand concentration in O<sub>2</sub> binding to hemoglobin (44). It should not come then as a surprise that active configurations formed by cooperative adsorbate binding like the zigzag O-decorated steps are present under the reacting conditions of catalysts and that such effects can be recognized by their nonlinear dependence on adsorbate concentration. There is also reason to believe that such active configurations are important in high pressure, high temperature reactors. First-principles statistical mechanics calculations of equilibrium structures have shown that O-decorated Pd step structures similar to those of this work are thermodynamically stable at high temperatures and pressures (45). We speculate that such active configurations caused by cooperative adsorbate interactions may play an essential role in many examples of real-world catalysis.

#### **References and Notes**

5

10

15

20

25

30

- J. W. Döbereiner, Neu entdeckte merkwürdige Eigenschaften des Suboxyds des Platins, des oxydirten Schwefel-Platins und des metallischen Platin Staubes. *Annalen der Physik* **74**, 269-273 (1823).
  - 2. J. W. Döbereiner, Platin und Wasserstoffgas. *Isis encyclopädische Zeitschrift, vorzügl. für Naturgeschichte, vergleichende Anatomie u. Physiologie*, 989-990 (1823).
  - 3. K. Nose, T. H. Okabe, in *Treatise on Process Metallurgy*. (2014), vol. 3: Industrial Processes, pp. 1071-1097.
  - 4. G. Busca, L. Lietti, G. Ramis, F. Berti, Chemical and mechanistic aspects of the selective catalytic reduction of NO<sub>x</sub> by ammonia over oxide catalysts: A review. *Applied Catalysis B-Environmental* **18**, 1-36 (1998).

5. J. Wang, H. Chen, Z. Hu, M. Yao, Y. Li, A Review on the Pd-Based Three-Way Catalyst. *Catalysis Reviews* **57**, 79-144 (2015).

5

10

15

25

- 6. S. Yun, S. T. Oyama, Correlations in palladium membranes for hydrogen separation: A review. *Journal of Membrane Science* **375**, 28-45 (2011).
- 7. S. N. Paglieri, J. D. Way, Innovations in palladium membrane research. *Separation and Purification Methods* **31**, 1-169 (2002).
- 8. M. Shao, Palladium-based electrocatalysts for hydrogen oxidation and oxygen reduction reactions. *Journal of Power Sources* **196**, 2433-2444 (2011).
- 9. E. Antolini, Palladium in fuel cell catalysis. *Energy & Environmental Science* **2**, 915 931 (2009).
- 10. M. V. Pagliaro *et al.*, Improving Alkaline Hydrogen Oxidation Activity of Palladium through Interactions with Transition-Metal Oxides. *ACS Catalysis* **12**, 10894-10904 (2022).
- 11. A. Russell, W. S. Epling, Diesel Oxidation Catalysts. *Catalysis Reviews* **53**, 337-423 (2011).
- 12. T. Lan *et al.*, Selective catalytic oxidation of NH<sub>3</sub> over noble metal-based catalysts: state of the art and future prospects. *Catalysis Science & Technology* **10**, 5792-5810 (2020).
- 13. B. S. Haynes, Combustion research for chemical processing. *Proceedings of the Combustion Institute* **37**, 1-32 (2019).
- F. Kuhlmann, Pour la fabrication de l'acide nitrique et des nitrates. *Patent No. FR11331*, (1838).
  - 15. W. Ostwald, Improvements in the Manufacture of Nitric Acid and Nitrogen Oxides. *Patent No. GB190200698A*, (1902).
  - 16. S. Dahl *et al.*, Role of steps in N<sub>2</sub> activation on Ru(0001). *Physical Review Letters* **83**, 1814-1817 (1999).
  - 17. J. Neugebohren *et al.*, Velocity-resolved kinetics of site-specific carbon monoxide oxidation on platinum surfaces. *Nature* **558**, 280-283 (2018).
  - 18. T. Zambelli, J. Wintterlin, J. Trost, G. Ertl, Identification of the "active sites" of a surface-catalyzed reaction. *Science* **273**, 1688-1690 (1996).
- 19. C. J. Weststrate, J. W. Niemantsverdriet, CO as a Promoting Spectator Species of C<sub>x</sub>H<sub>y</sub> Conversions Relevant for Fischer-Tropsch Chain Growth on Cobalt: Evidence from Temperature-Programmed Reaction and Reflection Absorption Infrared Spectroscopy. *ACS Catalysis* **8**, 10826-10835 (2018).
  - 20. M. Zhuo, A. Borgna, M. Saeys, Effect of the CO coverage on the Fischer-Tropsch synthesis mechanism on cobalt catalysts. *J Catal* **297**, 217-226 (2013).
  - 21. K. Reuter, C. Stampfl, M. V. Ganduglia-Pirovano, M. Scheffler, Atomistic description of oxide formation on metal surfaces: the example of ruthenium. *Chemical Physics Letters* **352**, 311-317 (2002).
- K. Reuter, M. Scheffler, First-principles kinetic Monte Carlo simulations for heterogeneous catalysis: Application to the CO oxidation at RuO<sub>2</sub>(110). *Physical Review B* 73, 045433 (2006).
  - 23. Y.-G. Wang, D. Mei, V.-A. Glezakou, J. Li, R. Rousseau, Dynamic formation of single-atom catalytic active sites on ceria-supported gold nanoparticles. *Nature Communications* **6**, 6511 (2015).
- 45 Z. Zhang, B. Zandkarimi, A. N. Alexandrova, Ensembles of Metastable States Govern Heterogeneous Catalysis on Dynamic Interfaces. *Accounts of Chemical Research* **53**, 447-458 (2020).

- 25. T. Zambelli, J. V. Barth, J. Wintterlin, G. Ertl, Complex pathways in dissociative adsorption of oxygen on platinum. *Nature* **390**, 495-497 (1997).
- 26. J. Neugebohren *et al.*, Velocity-resolved kinetics of site-specific carbon monoxide oxidation on platinum surfaces. *Nature* **558**, 280 283 (2018).

5

10

15

20

35

40

- 27. G. B. Park *et al.*, The kinetics of elementary thermal reactions in heterogeneous catalysis. *Nature Reviews Chemistry* **3**, 723-732 (2019).
- 28. I. Langmuir, A chemically active modification of hydrogen. *Journal of the American Chemical Society* **34**, 1310-1325 (1912).
- 29. I. Langmuir, Chemical reactions at very low pressures. I. The clean-up of oxygen in a tungsten lamp. *Journal of the American Chemical Society* **35**, 105-127 (1913).
- 30. I. Langmuir, The mechanism of the catalytic action of platinum in the reactions  $2CO + O_2 = 2CO_2$  and  $2H_2 + O_2 = 2H_2O$ . Transactions of the Faraday Society 17, 621 (1922).
- 31. T. Engel, H. Kuipers, Molecular-Beam Investigation of the Reaction  $H_2+1/2$   $O_2-> H_2O$  on Pd(111). Surf. Sci. **90**, 181-196 (1979).
- 32. T. Mitsui, M. K. Rose, E. Fomin, D. F. Ogletree, M. Salmeron, A scanning tunneling microscopy study of the reaction between hydrogen and oxygen to form water on Pd(111). *The Journal of Chemical Physics* **117**, 5855-5858 (2002).
  - 33. J. Fogelberg, L. G. Petersson, Kinetic modelling of the H<sub>2</sub>-O<sub>2</sub> reaction on Pd and of its influence on the hydrogen response of a hydrogen sensitive Pd metal-oxide-semiconductor device. *Surf. Sci.* **350**, 91-102 (1996).
  - 34. M. Jørgensen, H. Grönbeck, First-Principles Microkinetic Modeling of Methane Oxidation over Pd(100) and Pd(111). *ACS Catalysis* **6**, 6730-6738 (2016).
  - 35. D. C. Ford, A. U. Nilekar, Y. Xu, M. Mavrikakis, Partial and complete reduction of O2 by hydrogen on transition metal surfaces. *Surf. Sci.* **604**, 1565-1575 (2010).
- 25 M. J. Kratzer, J. Stettner, A. Winkler, Water Formation on Clean and Vanadium Oxide Covered Pd(111) by Permeating Deuterium. *The Journal of Physical Chemistry C* **111**, 12723-12729 (2007).
  - 37. R. Westerstrom *et al.*, Oxidation of Pd(553): From ultrahigh vacuum to atmospheric pressure. *Physical Review B* **76**, 155410 (2007).
- 38. F. Li *et al.*, Oxygen adsorption on stepped Pd(100) surfaces. *Surface Science* **604**, 1813-1819 (2010).
  - 39. C. T. Campbell, Future Directions and Industrial Perspectives Micro- and macro-kinetics: Their relationship in heterogeneous catalysis. *Topics in Catalysis* **1**, 353-366 (1994).
  - 40. C. T. Campbell, The Degree of Rate Control: A Powerful Tool for Catalysis Research. *ACS Catalysis* **7**, 2770-2779 (2017).
  - 41. S. Mallikarjun Sharada, T. Bligaard, A. C. Luntz, G.-J. Kroes, J. K. Nørskov, SBH10: A Benchmark Database of Barrier Heights on Transition Metal Surfaces. *The Journal of Physical Chemistry C* **121**, 19807-19815 (2017).
  - 42. M. I. Stefan, N. Le Novère, Cooperative Binding. *PLoS Computational Biology* **9**, e1003106 (2013).
  - 43. Q. Cui, M. Karplus, Allostery and cooperativity revisited. *Protein Science* **17**, 1295-1307 (2008).
  - 44. C. Bohr, K. Hasselbalch, A. Krogh, About a new biological relation of high importance that the blood carbonic acid tension exercises on its oxygen binding. *Skandinavisches Archiv Fur Physiologie* **16**, 402-412 (1904).
  - 45. Y. Zhang, K. Reuter, First-principles statistical mechanics approach to step decoration at surfaces. *Chemical Physics Letters* **465**, 303-306 (2008).

[SM references appear in the main file so that they link online. All references following ONE numbering sequence, use original number for any repeats from main list. Renumber the SM file references. Do NOT include a reference list in the SM as that list will NOT reflect our edits and the lists will not match. You note the references that appear only in the SM with the list of References at the end of the main =

1. C. R. Gebhardt, T. P. Rakitzis, P. C. Samartzis, V. Ladopoulos, T. N. Kitsopoulos, Slice imaging: A new approach to ion imaging and velocity mapping. *Review of Scientific Instruments* **72**, 3848-3853 (2001).

5

10

15

- 2. M. Schwarzer *et al.*, Adsorption and Absorption Energies of Hydrogen with Palladium. *J Phys Chem C* **126**, 14500-14508 (2022).
- 3. G. Kresse, J. Furthmüller, Efficiency of ab-initio total energy calculations for metals and semiconductors using a plane-wave basis set. *Computational Materials Science* **6**, 15-50 (1996).
- 4. G. Kresse, J. Furthmüller, Efficient iterative schemes for ab initio total-energy calculations using a plane-wave basis set. *Physical Review B* **54**, 11169-11186 (1996).
- 5. J. P. Perdew, K. Burke, M. Ernzerhof, Generalized gradient approximation made simple (vol 77, pg 3865, 1996). *Physical Review Letters* **78**, 1396-1396 (1997).
- 6. B. Hammer, L. B. Hansen, J. K. Norskov, Improved adsorption energetics within density-functional theory using revised Perdew-Burke-Ernzerhof functionals. *Physical Review B* **59**, 7413-7421 (1999).
  - 7. G. Kresse, D. Joubert, From ultrasoft pseudopotentials to the projector augmented-wave method. *Physical Review B* **59**, 1758-1775 (1999).
- 8. P. E. Blöchl, Projector augmented-wave method. *Physical review B* **50**, 17953 (1994).
  - 9. G. Henkelman, B. P. Uberuaga, H. Jónsson, A climbing image nudged elastic band method for finding saddle points and minimum energy paths. *The Journal of Chemical Physics* **113**, 9901-9904 (2000).
- 10. G. Henkelman, H. Jonsson, A dimer method for finding saddle points on high dimensional potential surfaces using only first derivatives. *Journal of Chemical Physics* **111**, 7010-7022 (1999).
  - 11. J. A. Herron, S. Tonelli, M. Mavrikakis, Atomic and molecular adsorption on Pd(111). *Surf. Sci.* **606**, 1670-1679 (2012).
  - 12. C. T. Campbell, Future Directions and Industrial Perspectives Micro- and macro-kinetics: Their relationship in heterogeneous catalysis. *Topics in Catalysis* **1**, 353-366 (1994).

- 13. C. T. Campbell, The Degree of Rate Control: A Powerful Tool for Catalysis Research. *ACS Catalysis* 7, 2770-2779 (2017).
- 14. S. Mallikarjun Sharada, T. Bligaard, A. C. Luntz, G.-J. Kroes, J. K. Nørskov, SBH10: A Benchmark Database of Barrier Heights on Transition Metal Surfaces. *The Journal of Physical Chemistry C* **121**, 19807-19815 (2017).
- 15. J. D. Cox, D. D. Wagman, V. A. Medvedev, *CODATA Key Values for Thermodynamics*. (Hemisphere Publishing Corp., New York, 1984), vol. 1.
- 16. M. Peter, S. Adamovsky, J. M. Flores Camacho, S. Schauermann, Energetics of elementary reaction steps relevant for CO oxidation: CO and O2 adsorption on model Pd nanoparticles and Pd(111). *Faraday Discussions* **162**, 341-354 (2013).
- 17. X. Guo, A. Hoffman, J. T. Yates, Jr., Adsorption kinetics and isotopic equilibration of oxygen adsorbed on the Pd(111) surface. *The Journal of Chemical Physics* **90**, 5787-5792 (1989).

# Acknowledgments

5

10

15

25

30

35

For the DFT calculations MS used the Center for Advanced Research Computing (CARC) at UNM, as well as the Scientific Compute Cluster at GWDG, the joint data center of Max Planck Society for the Advancement of Science (MPG) and University of Göttingen.

**Funding:** MS thanks the BENCh graduate school, funded by the DFG (389479699/GRK2455). MS, JF and TNK acknowledge support from the European Research Council (ERC) under the European Union's Horizon 2020 research and innovation programme (grant agreement no. [833404]). DB acknowledges support from the Alexander von Humboldt Foundation for financial support through a Feodor-Lynen Research Fellowship. YW and HG acknowledge support from the National Science Foundation (CHE-1951328 and CHE-2306975) and HG is a Humboldt Research Awardee. DJA acknowledges support from The International Center for Advanced Studies of Energy Conversion, D37077 Göttingen, Germany.

# **Author contributions:**

Conceptualization: M.S.(lead), D.B.(supporting), T.N.K.(supporting)

Methodology: M.S.(lead), D.B. (supporting), T.N.K. (supporting), A.M.W. (supporting)

Investigation: M.S. (lead), D.B. (supporting), J.F. (supporting), Y.W. (supporting)

Funding acquisition: A.M.W., T.N.K., H.G.

Supervision: A.M.W., T.N.K., H.G.

Writing – original draft: A.M.W., M.S.

Writing – review & editing: D.J.A., H.G., T.N.K., D.B., J.F.

# Submitted Manuscript: Confidential Template revised November 2022

Competing interests: Authors declare that they have no competing interests.

**Data and materials availability:** All data needed to evaluate the conclusions in the paper are present in the paper or the Supplementary Materials. (if need be, data sets can be deposited with Dryad or similar databases listed).

# **Supplementary Materials**

Materials and Methods

References (46-62)

Supplementary Text

5

Figs. S1 to S20

Tables S1 to S15